Digital algorithm for dispersion correction in optical coherence tomography for homogeneous and stratified media

Daniel L. Marks, Amy L. Oldenburg, J. Joshua Reynolds, and Stephen A. Boppart

The resolution of optical coherence tomography (OCT) often suffers from blurring caused by material dispersion. We present a numerical algorithm for computationally correcting the effect of material dispersion on OCT reflectance data for homogeneous and stratified media. This is experimentally demonstrated by correcting the image of a polydimethyl siloxane microfluidic structure and of glass slides. The algorithm can be implemented using the fast Fourier transform. With broad spectral bandwidths and highly dispersive media or thick objects, dispersion correction becomes increasingly important.

OCIS codes: 100.3010, 110.4500, 260.2030.

1. Introduction

In optical coherence tomography (OCT),[1–7] there are a number of factors that limit the practical resolution of the system. Finite bandwidth sources, dispersion,[8] uncertainty in material composition, strong scattering, absorption, and refraction can all have distorting effects on the measurements. Some of these nonidealities, such as absorption and scattering reduce the signal power that can be collected, while others such as dispersion and refraction alter the signal without power loss. For OCT imaging, one would like to achieve the best resolution given the available signal. Toward this aim, we present a detailed model of OCT to derive signal-processing formulas that can be used to enhance OCT images. These formulas are derived with simplicity and economy in mind so that they can be practically applied.

The practice of OCT often makes a number of assumptions that simplify OCT data acquisition and analysis, but in some cases can result in suboptimal imaging performance. OCT systems are typically implemented as Michelson interferometers with free-space or fiber optics, where one of the arms contains a sample to be measured, and the other contains a delay line that allows one to scan the relative time delay between the reference and sample signals. The sample arm often consists of mirrors to steer the beam through the sample, and a focusing objective to confine the beam to a narrow column. Ideally, the spot size of the beam determines the transverse resolution, while the coherence length of the source determines the axial resolution. Flaws in the optics of the system can reduce the performance of diffraction or bandwidth-limited imaging. Some of these flaws attenuate the signal, which cannot be recovered, while others distort the signal but preserve the signal power. By characterizing these distortions, it should be possible to perform a more detailed analysis of measured data and produce a refined image that approaches the quality of one acquired with an ideal apparatus.

One type of distortion that occurs frequently in OCT is dispersion. Dispersion occurs when the group velocity (or envelope speed) of an optical pulse is not constant in a material. In normal dispersion, the type usually encountered, low frequencies travel faster than high frequencies. A pulse traveling through such a medium tends to turn into a chirp where the signal increases in frequency as it passes a particular point in the medium. On an OCT image, this changes a formerly sharp point into a blurred

D. L. Marks, A. L. Oldenburg, and J. J. Reynolds are with the Department of Electrical and Computer Engineering, Beckman Institute of Advanced Science and Technology, University of Illinois at Urbana-Champaign. S. A. Boppart (boppart@uiuc.edu) is with the Department of Electrical and Computer Engineering, Bioengineering Program, Beckman Institute for Advanced Science and Technology, College of Medicine, University of Illinois at Urbana-Champaign, 405 N. Mathews Avenue, Urbana, IL 61801.
Received 8 April 2002; revised manuscript received 26 September 2002.
0003-6935/03/020204-14$15.00/0

region within an axial scan. As the pulse propagates along, it lengthens, and subsequently the axial resolution decreases. However, dispersion itself does not change the amount of signal captured by the detector.

There have been other approaches to digital dispersion correction. A similar approach to that presented here uses a resampling technique for homogeneous waveguides.[9,10] Another method uses a space-variant convolution kernel to correct dispersion in OCT images.[11] This method, most related to ours, corrects dispersion by convolving the signal at various points on the axial scan by a point spread function with the conjugate phase to the dispersion. While this can correct space-variant dispersion, it is using a space-invariant kernel and therefore corrects only one depth per convolution. Other related methods use complex-domain methods to correct phase aberrations and speckle and an optical quadrature-phase measurement technique to directly sample the complex analytic signal.[12] A method by use of the clean algorithm from astronomy to estimate the position of scatterers in a medium has been proposed and demonstrated.[13] Two other studies have explored limits to imaging quality imposed by the scattering properties of the medium.[14,15] A unique method of dispersion correction utilizes photon entanglement to automatically cancel dispersion.[16] In this work, the limits imposed by dispersion of the medium and the photodetection process are investigated. The two effects are investigated together because each contribution to the image formation can be separated cleanly. Dispersion is a linear, power-preserving distortion that can be digitally corrected, while photodetection limits fundamentally prevent accurate recovery of the signal.

In particular, dispersion correction and accounting for a nonuniform spectrum signal become important when the bandwidth of the illumination signal becomes extremely large. To study subcellular biological structures, imaging resolutions will be needed that are on the order of the size of the wavelength of light. At a large fractional bandwidth, dispersion increasingly degrades image quality. Dispersion can easily be optically corrected at one depth by balancing the dispersion between the sample and the reference arms. However, correcting the dispersion over a wide-depth scanning range can be very challenging. The state-of-the-art sources[17–21] have very large fractional bandwidth, and a digital method of dispersion compensation would be advantageous to simplify data acquisition. The method and algorithm presented here attempts to form an estimate of the scatterer distribution in a medium, accounting for dispersion and nonuniform detector response and spectrum. It applies to both homogeneous and stratified media, and is presented in both full and simplified form depending on the complexity of the inversion process desired. This algorithm accounts for the dispersion of the medium and the delay mechanism, the amount of power returned from the sample, the detector quantum efficiency and bandwidth, and the shape and bandwidth of the source spectrum, all of which influence reconstruction quality.

A model of signal detection in OCT presented in Section 2 is required to discuss the multiple factors, their effects, and how they can be accounted for. This model describes the dispersing and scattering medium, the potential imperfections of the delay mechanism, the illumination source, and the photodetection limits. This model is applied to dispersion correction in a homogeneous medium in Section 3. From these models a linear least squares estimate of the scattering function of the medium is formed. Section 4 describes how, by use of a homogeneous slab of the medium, the dispersion of the medium and the delay line can be jointly characterized. The dispersion compensation method is extended to multiple layers of homogeneous media in Section 5. The demodulation of the scattering amplitude and its effect on speckle is discussed in Section 6, and an experimental demonstration of these techniques is presented in Section 7. Discussions and conclusions are drawn in Sections 8 and 9, respectively.

2. Model of Optical Coherence Tomography Detection

Consider a semi-infinite one-dimensional medium, with a reflectance function $g(z)$ that is nonzero for $z > 0$. This medium is not necessarily homogeneous in content, and only singly backscattered light is considered. Incident on this medium is a scalar signal random process $f(t)$ that is wide-sense stationary with power spectral density $\tilde{S}(\omega)$. The medium will be characterized by a real-valued phase retardance function $\phi_S(z, \omega)$, which is the total phase retardance encountered by a signal of frequency ω after traveling a distance z into the material, reflecting off a delta-function scatterer at that depth, and returning a distance z. Assume that the material has a real response, so that $\phi_S(z, -\omega) = -\phi_S(z, \omega)$. The cross-spectral density $\tilde{W}(\omega)$ between the incident and the reflected signals will then be:

$$\tilde{W}(\omega) = \tilde{S}(\omega) \int_0^\infty \exp[i\phi_S(z, \omega)]g(z)\mathrm{d}z. \qquad (1)$$

Note that this model is unrealistic because it does not account for the absorption of the medium. Because of causality (as characterized in the Kramers–Kronig relations[22]), dispersion at a given frequency must be accompanied by absorption. Without absorption, the phase delay produced at a given scatterer in the medium will not be causal. Therefore a portion of the wave incident on the scatterer would falsely appear at a shallower depth. If the absorption is weak (occurring over many wavelengths), then the fraction of the wave that is advanced to shallower depths is small and can be neglected. In this work the effect of absorption is neglected and the anticausal advance produced by Eq. (1) is assumed to be small.

OCT systems also require a delay mechanism that allows one to vary the relative delay between a ref-

erence and signal arm. This delay mechanism will be characterized by a parameter t, which could be mirror position, acousto-optical driving frequency, or some other quantity that is varied continuously while scanning an axial line. A similar phase-delay function $\phi_D(t, \omega)$ will characterize the phase retardance produced on a frequency ω when the delay line is at position t. The cross-spectral density between the incoming illumination $\tilde{S}(\omega)$ and the delayed signal $\tilde{W}_D(t, \omega)$ will be

$$\tilde{W}_D(t, \omega) = \tilde{S}(\omega)\exp[i\phi_D(t, \omega)]. \quad (2)$$

The wide-sense stationary signals returning from the delay arm and the sample arm will be summed together, and the intensity will be integrated on a photodetector. If the quantum efficiency of the detector is $\eta(\omega)$ at frequency ω, the total photocount $P(t)\Delta t$ the photodetector receives over an interval Δt will be given by

$$P(t)\Delta t = \text{Poisson}\left[R\Delta t + \frac{\Delta t}{2\pi}\int_{-\infty}^{\infty}\frac{I(t, \omega)\eta(\omega)}{\hbar\omega}\,\mathrm{d}\omega\right]$$

where

$$I(t, \omega) = \tilde{S}(\omega) + \frac{|\tilde{W}(\omega)|^2}{\tilde{S}(\omega)} + 2\mathrm{Re}\{\tilde{W}(\omega)\exp[-i\phi_D(t, \omega)]\}. \quad (3)$$

The operator Poisson indicates that the argument is the parameter to a Poisson random process that produces a discrete number of photocounts based on its argument. The variable R is a thermal photocount rate that occurs independent of the incoming intensity. The intensity $I(t, \omega)$ has a background term that is independent of t: $\tilde{S}(\omega) + |\tilde{W}(\omega)|^2/\tilde{S}(\omega)$. This background term is usually of no interest because the interferometric data is high frequency. It is typically discarded by subtracting off the average of the photocount $P(t)$ over t. Once the background level is known, there is a linear relationship between the photocount $P(t)$ and the cross-spectral density $\tilde{W}(\omega)$. One can then use an iterative scheme, such as the Richardson–Lucy[23] maximum likelihood algorithm to estimate $\mathrm{Re}\{\tilde{W}(\omega)\}$ from $P(t)$ assuming Poisson noise. The methods presented in this work can be used to increase the speed of an iterative restoration algorithm, but this approach is not pursued here.

Except for the background level, the photocount $P(t)$ is a real, positive signal consisting of high-frequency content. Therefore the complex analytic signal[24,25] $P_A(t)$ can be found from the photocount $P(t)$ using the Hilbert transform (or its Fourier equivalent). If the background photocount rate is given by B, and we neglect the random nature of $P(t)$ as a Poisson process, then the relationship between $P(t)$ and $\tilde{W}(\omega)$ is given by

$$P_A(t)\Delta t = B\Delta t + \frac{\Delta t}{\pi}\int_0^{\infty}\frac{\tilde{W}(\omega)\eta(\omega)}{\hbar\omega}\exp[-i\phi_D(t, \omega)]\mathrm{d}\omega$$

where

$$B = R + \frac{1}{2\pi}\int_{-\infty}^{\infty}\frac{\eta(\omega)\left[\tilde{S}(\omega) + \dfrac{|\tilde{W}(\omega)|^2}{\tilde{S}(\omega)}\right]}{\hbar\omega}\,\mathrm{d}\omega. \quad (4)$$

This is an integral of similar form to Eq. (1), replacing z in Eq. (1) by ω, ω in Eq. (1) by t, $\phi_S(z, \omega)$ with $-\phi_D(t, \omega)$, $\tilde{W}(\omega)$ by $P_A(t)$, and $g(z)$ by $\tilde{W}(\omega)\eta(\omega)/\hbar\omega$. This work presents a way to numerically perform an approximation of these integrals in some cases using the fast Fourier transform (FFT). Because there are actually two of these integrals, one to compute the cross-spectral density $\tilde{W}(\omega)$ from the photocount $P(t)$, and another to compute the scattering density $g(z)$ from $\tilde{W}(\omega)$, the method will be applied twice. Applying these methods can account for the nonidealities of the delay line or materials used in OCT.

3. Dispersion Correction in a Homogeneous Medium

When the space $z > 0$ is filled with a homogeneous medium the equations are simplified. The medium has a dispersion function $k(\omega)$ that is an increasing or decreasing function of ω, and the useful bandwidth of the system occurs between $\omega_0 - \Delta\omega < \omega < \omega_0 + \Delta\omega$ (as determined by the bandwidth of the illumination). In this case, the phase retardance of the medium $\phi_S(z, \omega) = 2zk(\omega)$, and Eq. (1) becomes

$$\tilde{W}(\omega) = \tilde{S}(\omega)\int_0^{\infty}\exp[2ik(\omega)z]g(z)\mathrm{d}z. \quad (5)$$

By changing the variables $k = k(\omega)$, this becomes a Fourier integral:

$$\tilde{W}(k) = \tilde{S}(k)\int_0^{\infty}\exp(2ikz)g(z)\mathrm{d}z. \quad (6)$$

This resampling suggests a way to recover an estimate of the scattering density $g(z)$ from the cross-spectral density $\tilde{W}(k)$. First, find the cross-spectral density normalized by the illumination spectrum: $\tilde{G}(k) = \tilde{W}(k)/\tilde{S}(k)$. Then, take the inverse Fourier transform of $\tilde{G}(k)$ to find $g(z)$. This corrected $g(z)$ should have all of the dispersion compensated as a function of depth. Because the Fourier transform steps can be accomplished efficiently by the FFT, the only difficult step is finding $\tilde{W}(k)$ from $\tilde{W}(\omega)$. Because OCT often requires detection of very faint reflections from deep objects, inaccuracy of the resampling in the Fourier domain can directly limit the quality of the reconstruction at larger depths (because there is usually exponentially less reflectance from them).

Note that the estimate of the normalized cross-spectral density $\tilde{G}(k) = \tilde{W}(k)/\tilde{S}(k)$ will in general be numerically unstable because when illumination spectral density $\tilde{S}(k)$ is small, noise will dominate the reconstruction at those frequencies. It is desirable to use an estimator for $\tilde{G}(k)$ that accounts for the noise, in this case chiefly Poisson noise. To do this,

consider that the photodetector receives photons at an average rate of B. The photocount measurements are N samples of the photon counts during adjacent nonoverlapping intervals of length Δt on the photodetector. The coherence time of the source is very short. Therefore the covariance of the photon count between all of the intervals is zero. Because of this, the Poisson random variable of parameter $B\Delta t$ in each interval is approximated by an independent Gaussian random variable of mean and variance $B\Delta t$. The photon noise then acts as a discrete-time white-noise process of average power $B\Delta t$.

If the phase retardance $\phi_D(t, \omega)$ is that of a delay line, Eq. (3) implements a linear transformation similar to that of a Fourier transform. Because the photon noise component of adjacent samples of the photon counts are uncorrelated, the Fourier transform would distribute the shot noise due to the $BN\Delta t$ photons incident on the detector equally among all of the frequency components within the maximum measured optical frequency rate of the system, called ω_{max}. The frequency ω_{max} is determined by the sampling rate in the variable t. The variance in the number of photons per unit bandwidth due to noise will be $\mathrm{Var}[\tilde{P}_N(\omega)] = BT/\omega_{max}^2$, where $T = N\Delta t$, or the total integration time per axial scan.

To estimate the variance in the photocurrent due to the reflection from the sample itself, assume that the spectrum from the sample is a modulated version of the spectrum from the illumination source. This *a priori* condition can be violated in cases, for example, where the observed object are periodic structures like Bragg gratings (and therefore changes the return spectrum very nonuniformly). For most objects without periodicity, this condition should work reasonably well. Only a fraction of the input power will be returned from the sample, a fraction denoted by γ. Weighted by this fraction and quantum efficiency, the variance in the number of signal photons will be given by $\mathrm{Var}[\tilde{P}_S(\omega)] = 2\gamma[\tilde{S}(\omega)\eta(\omega)T/\hbar\omega]^2$. By use of the linear-least-squares estimator, the estimate of the true number of photons per unit bandwidth will be

$$\tilde{P}_E(\omega) = \frac{\tilde{P}(\omega)\mathrm{Var}[\tilde{P}_S(\omega)]}{\mathrm{Var}[\tilde{P}_S(\omega)] + \mathrm{Var}[\tilde{P}_N(\omega)]} = \frac{\tilde{P}(\omega)2\gamma\tilde{S}(\omega)^2}{2\gamma\tilde{S}(\omega)^2 + \dfrac{B(\hbar\omega)^2}{T\eta(\omega)^2\omega_{max}^2}}. \quad (7)$$

The background photocount B $\tilde{P}(\omega)$ is removed from the measured photocount when one computes $\tilde{P}(\omega)$ from $P_A(t)$ using Eq. (4). Accounting for the quantum efficiency of the photodetector, the estimate of the cross-spectral density is $\tilde{W}(\omega) = \tilde{P}_E(\omega)\hbar\omega/\eta(\omega)$. The estimate of normalized spectral density $\tilde{G}(\omega)$ becomes

$$\tilde{G}(\omega) = \frac{\tilde{W}(\omega)2\gamma\tilde{S}(\omega)}{2\gamma\tilde{S}(\omega)^2 + \dfrac{B(\hbar\omega)^2}{T\eta(\omega)^2\,\omega_{max}^2}}. \quad (8)$$

Eq. (8) is actually the expression for a Wiener filter on the signal $\tilde{W}(\omega)$ with the filter having the frequency response $\tilde{S}(\omega)$, and noise power-spectral-density $N(\omega) = [(\hbar\omega)^2B/\eta(\omega)^2\omega_{max}^2T]$. This is because the spectrum of the actual source can be regarded as a filter to a uniform spectrum source placed before the photodetector. The noise spectral density is not a true spectral density (because it is not time independent), but can be used like one over a finite time interval T when the Poisson process is partitioned into intervals of length Δt to achieve a sampling rate of ω_{max}. As the integration time grows, this pseudo-spectral density decreases because there are more photons collected per spectral channel. Since $N(\omega)$ may vary slowly over the bandwidth of interest, it may be sufficient to replace $N(\omega)$ by a constant that can be estimated from the signal itself, perhaps from ranges of optical frequencies that are known to be outside the spectrum emitted by the illumination source.

There is a seemingly incorrect conclusion one could draw from Eq. (8). Namely, that the noise can be made arbitrarily low by making ω_{max} as large as possible by sampling in the variable t as finely as possible. This conclusion is valid, until the sampling time Δt is reduced to the coherence time of the optical field. With further reduction of Δt, the assumption that the adjacent measurements of the photocount have zero covariance is strongly violated, and so no new information is obtained by reducing the sampling time Δt further. Because photons can arrive at any instant, the photon noise creates frequencies that are aliased into the estimates of the reflectances at optical frequencies that are actually present in the signal. As Δt is decreased, the aliasing decreases and therefore less of this randomness is present in the reconstructed signal. Alternately, one could use an analog anti-aliasing filter (a function that is usually implemented by the finite response time of the photodetector). Note, however, that the Gaussian approximation to the Poisson distribution may not work well when the number of photons captured in the interval Δt is low (on the order of one photon or fewer), which is usually not the case for most relatively slow photodetector temporal responses.

If the cross-spectral density $\tilde{W}(\omega)$ is known, one can compute the Wiener filter estimate of the normalized cross-spectral density $\tilde{G}(\omega)$, use a resampling interpolator to compute $\tilde{G}(k)$, and then use the FFT to estimate $g(z)$ from these samples. When utilizing an interpolation scheme, one must make *a priori* assumptions about the nature of the sampled function. For example, one can assume it is a bandlimited function. Because interpolation is occurring in the Fourier domain, using a bandlimiting interpolator actually makes assumptions about the interval of time that the function $\tilde{G}(\omega)$ occupies. Because there is a practical limit on the depth or range over which OCT can scan, this time interval can be taken as the time limit to use in the interpolation algorithm. An overestimated time limit will result in more terms

being required to compute the interpolated points, but should not change the estimate.

A similar method can be employed to estimate the cross-spectral density $\tilde{W}(\omega)$ from the photocount $P(t)$. For now, assume that the dispersion function of the delay line $\phi_D(t, \omega) = \phi_0(\omega) + r(t)\phi_1(\omega)$, and that $r(t)$ and $\phi_1(\omega)$ are increasing or decreasing functions of their respective arguments. This form of the delay-line dispersion has been chosen because it is the most general form that can be corrected with two resamplings and the Fourier transform. In this form, the function $\phi_0(\omega)$ represents the fixed dispersion between the delay mechanism and the sample arm of the interferometer. Typically, this is caused by an extra length of optical fiber or thicker glass in one interferometer arm. The second term, $\phi_1(\omega)$, represents nonlinearity of the application of the delay as a function of frequency that occurs, for example, because the delay line is embedded in a medium with dispersion (a movable mirror in a liquid). This term can be adjusted to correct the dispersion caused by Fourier-transform delay lines. The term $r(t)$ compensates for the nonlinearity of the mirror in time. For example, this can be the nonlinearity caused by the motion of a delay arm in a circular arc or with a sinusoidal velocity rather than at a constant velocity. With these assumptions of the form of the delay-line dispersion, Eq. (4) becomes

$$P_A(t) = B + \frac{1}{\pi}\int_{\omega_0-\Delta\omega}^{\omega_0+\Delta\omega} \frac{\tilde{W}(\omega)\eta(\omega)}{\hbar\omega} \exp[-i\phi_0(\omega) - ir(t)\phi_1(\omega)]d\omega. \quad (9)$$

After defining new variables $t' = r(t)$ and $\beta = \phi_1(\omega)$, this again becomes a Fourier integral:

$$P_A(t') = B + \frac{1}{\pi}\int_{\phi_1(\omega_0-\Delta\omega)}^{\phi_1(\omega_0+\Delta\omega)} \tilde{P}_\beta(\beta)\exp(-it'\beta)d\beta$$

where

$$\tilde{P}_\beta(\beta) = \tilde{W}[\phi_1^{-1}(\beta)]\eta[\phi_1^{-1}(\beta)] \times \left[\hbar\phi_1^{-1}(\beta)\frac{d\beta}{d\omega}\right]^{-1} \exp\{-i\phi_0[\phi_1^{-1}(\beta)]\}. \quad (10)$$

This suggests that a method of recovering the cross-spectral density $\tilde{W}(\omega)$ from the photocount $P(t)$ would be to first resample $P(t)$ to $P(t')$, compute the complex analytic signal $P_A(t')$ from $P(t')$, take its Fourier transform to find $\tilde{P}_\beta(\beta)$, and multiply by $\eta[\phi_1^{-1}(\beta)]^{-1}\hbar\phi_1^{-1}(\beta)(d\beta/d\omega)\exp\{i\phi_0[\phi_1^{-1}(\beta)]\}$ to find $\tilde{W}(\beta)$. The result then can be resampled to find $\tilde{W}(\omega)$. This is similar to the procedure for Eq. (6), except interpolation occurs on both variables t and ω. If a bandlimiting interpolator were to be used for both, this would require that the function have limited intervals in both t and ω. However, because both t and ω are Fourier conjugate variables, they cannot both be limited. These variables can be approximately specified to be in finite intervals if the actual time-bandwidth product (in t and ω space) that the signal occupies is significantly less than the time-bandwidth product of the sampling system. This is usually the case if the signal is oversampled in both the time and the frequency domain.

Instead of finding $\tilde{W}_\beta(\beta)$ first, which requires resampling the quantum efficiency $\eta(\omega)$ and the dispersion $\phi_0(\omega)$ to the β variable, effort is saved by first resampling the $\tilde{P}_\beta(\beta)$ to the ω variable, which is the photocount $\tilde{P}(\omega)$. This process incorporates the Jacobian factor $d\beta/d\omega$ to preserve the total signal energy. Then the cross-spectral density $\tilde{W}(\omega)$ equals $\tilde{P}(\omega)\hbar\omega/\eta(\omega)$.

The required period in t can be estimated that prevents aliasing. Define β_{max} as the larger of $\phi_1(\omega_0 - \Delta\omega)$ and $\phi_1(\omega_0 + \Delta\omega)$. The sampling period in t' should be π/β_{max}. The maximum sampling period in t required will then be $\Delta t = \pi/[\beta_{max}|dt'/dt|_{max}]$. The sampling rate in z can be computed by defining k_{max} as the larger of $k(\omega_0 - \Delta\omega)$ and $k(\omega_0 + \Delta\omega)$, with $\Delta z = \pi/2k_{max}$. These are approximate conditions because a resampled version of a bandlimited function is not necessarily bandlimited, and therefore some aliasing may be inevitable. However, if $r(t)$ is slowly varying, the amount of power outside the band should be negligible.

The two steps can be combined to form a complete algorithm for inverting OCT reflectance data in a homogeneous medium, as shown in Table 1. A resampling step can be eliminated by performing the Wiener filter in the k variable rather than in the ω variable. To do this, the cross-spectral density $\tilde{W}(\beta)$ should be resampled directly to $\tilde{W}(k)$ in Step 4, followed by the use of the Wiener filter in Step 5 in the k variable. To do this, the noise spectral density must be resampled from $N(\omega)$ to $N(k)$. When resampling is performed, the proper Jacobian $dk/d\omega$ should be used to preserve the total noise power in the signal. In Step 2, the Fourier transform inherently computes the complex analytic signal, and so no explicit Hilbert transform step is needed.

The above procedure requires knowledge of many details of the optical system: $r(t)$, $\eta(\omega)$, $\tilde{S}(\omega)$, $\phi_0(\omega)$, $\phi_1(\omega)$, and $k(\omega)$. In particular, measuring $\phi_0(\omega)$ and $\phi_1(\omega)$ will require an absolute time reference or delay line. In practice a simpler algorithm is often preferred at the expense of some image reconstruction fidelity, because achieving all of the benefits of an improved algorithm often requires thorough and precise measurement of these parameters. If only dispersion correction is required, without compensating for the noise or source spectral characteristics, this procedure can be simplified greatly.

To simplify this procedure, note that in Step 3, the functions $\eta[\phi_1^{-1}(\beta)]^{-1}$, $\hbar\phi_1^{-1}(\beta)$, and $(d\beta/d\omega)$ are real functions that tend to be slowly varying over the fractional bandwidth utilized in the signal. They act as windowing functions that minimally change the point spread function. Therefore one may omit these terms with no significant effects. In Step 5, if

Table 1. Algorithm for Dispersion Correction in a Homogeneous Medium

1. Resample the measurements $P(t)$ to $P(t')$ by use of the relation $t' = r(t)$.
2. Take the Fourier Transform (via the FFT) of $P(t')$ to find $\tilde{P}_\beta(\beta)$. This produces the complex analytic signal because the negative frequencies will be ignored.
3. Resample $\tilde{P}_\beta(\beta)$ to $\tilde{P}(\omega)$ using the relation $\beta = \phi_1(\omega)$ and the Jacobian factor $\frac{d\beta}{d\omega}$.
4. Compute $\tilde{W}(\omega) = \tilde{P}(\omega)\exp(i\phi_0(\omega))\frac{\hbar\omega}{\eta(\omega)}$.
5. Compute $\tilde{G}(\omega) = \frac{2\tilde{W}(\omega)\gamma\tilde{S}(\omega)}{2\gamma\tilde{S}(\omega)^2 + N(\omega)}$.
6. Resample $\tilde{G}(\omega)$ to find $\tilde{G}(k)$ by using the relation $k = k(\omega)$ and the Jacobian $dk/d\omega$.
7. Take the inverse Fourier transform of $\tilde{G}(k)$ to yield $g(2z)$.

one neglects noise and assumes that the spectrum of the source is uniform, then $\tilde{G}(k) \approx \tilde{W}(k)$, a typical approximation made in OCT.

The need to explicitly determine $\phi_0(\omega)$, $\phi_1(\omega)$, and $k(\omega)$ can also be removed. Instead, $\phi_0[\phi_1^{-1}(\beta)]$ that is abbreviated $\phi_0(\beta)$ can be measured and used directly in Step 3. The function $k[\phi_1^{-1}(\beta)]$ can similarly be measured directly [and is now called $k(\beta)$]. By performing these measurements, there is no longer a need to specify $\phi_1(\omega)$. The simplified method is summarized in Table 2.

Three functions remain to be determined: the delay-motion nonlinearity $r(t)$, the fixed dispersion $\phi_0(\beta)$, and the medium dispersion $k(\beta)$. With those determined, the medium dispersion can be simultaneously characterized without a reference delay line. In practice, these three functions can be approximated accurately by polynomials of the second order. In a nondispersive system, all functions would be linear. However, the higher-order correction terms, albeit small, influence image quality.

If the quadratic approximation is used for these three functions, then only the ratio of the quadratic and linear coefficients affect image quality. The absolute magnitude of the functions $r(t)$ and $k(\beta)$, which are used to resample, only affect the scale of the reconstruction and not the quality. The absolute magnitude of $\phi_0(\beta)$ only affects the position of the reconstruction (because it is a linear phase). Maintaining image quality therefore depends on measuring the ratio of the quadratic and linear coefficients for these three functions, requiring only three parameters to be measured or fit to the data.

4. Calibration of Parameters by Use of a Homogeneous Slab

While the dispersion of the material and of the delay arm may be difficult to measure separately without a witness dispersion-free delay mechanism, the combined dispersion can easily be measured together and can be used to correct both the dispersion of the material and the delay arm simultaneously.

Assume that a homogeneous slab of the medium has two parallel surfaces. The slab must be sufficiently thick to introduce a measurable chirp. When the optical signal is sent into the slab, reflections off the near and the far surfaces (through the medium) will be produced. When an optical signal is sent through the medium, a reflectance signal photocount $P(t)$ is measured for $t_1 < t < t_2$. All of the chirp on the front reflection will be due to the delay mechanism, while the back reflection will have dispersion due to both the delay mechanism and the material. Assume that the chirp in the medium is not so extreme that there exists a delay value t_0 such that the entire signal $P(t)$ for $t < t_0$ is due to the front reflection, and the back surface reflection is confined to $t > t_0$.

From $P(t)$, two functions can be defined $P_i(t)$ that equals $P(t)$ for $t < t_0$ and zero otherwise, and $P_r(t)$ that equals $P(t)$ for $t > t_0$ and zero otherwise. A function can be determined that simultaneously characterizes the spectrum of the source and the dispersion not due to the medium:

$$\tilde{W}_i(\beta) = \int_{t_1}^{t_0} P(t)\exp(i\beta r(t))\mathrm{d}t,$$

$$\tilde{W}_r(\beta) = \int_{t_0}^{t_2} P(t)\exp(i\beta r(t))\mathrm{d}t. \qquad (11)$$

The spectrum $\tilde{W}_i(\beta)$ contains the spectral characteristics of the illumination and the chirp introduced by the delay line. Ideally, this reflection is from a single surface and therefore should not introduce any

Table 2. Algorithm for Dispersion Correction in a Homogeneous Medium without Noise Compensation

1. Resample the measurements $P(t)$ to $P(t')$ by using the relation $t' = r(t)$.
2. Take the Fourier transform (via the FFT) of $P(t')$ to find $\tilde{P}_\beta(\beta)$. This produces the complex analytic signal because the negative frequencies will be ignored.
3. Multiply $\tilde{P}_\beta(\beta)$ by $\exp[i\phi_0(\beta)]$ to find $\tilde{W}(\beta)$.
4. Resample $\tilde{W}(\beta)$ to find $\tilde{W}(k)$ using the relation $k = k(\beta)$.
5. Take the inverse Fourier transform of $\tilde{W}(k)$ to yield $g(2z)$.

Table 3. Algorithm for Dispersion Correction in a Stratified Medium

1. Resample $\tilde{G}(\omega)$ to $\tilde{G}(k)$ by using the relation $k = k_i(\omega)$.
2. Take the inverse Fourier transform (via the FFT) to find $g_i(z)$.
3. Extract the region $0 < z < z_{i+1} - z_i$ out of $g_i(z)$ and then set the region of the function to zero.
4. Take the Fourier transform (via the FFT) to find $\tilde{G}'(k)$.
5. Resample $\tilde{G}'(k)$ to $\tilde{G}'(\omega)$ by using the relation $k = k_i(\omega)$.
6. Set the new $\tilde{G}(\omega) = \tilde{G}'(\omega)\exp[-i(z_i - z_{i-1})k_i(\omega)]$.
7. Increment i by one and go back to step 1 until $i > N$.

chirp or variation in the spectrum if illuminated by a uniform spectrum source. From this, an estimate can be formed of the phase shift produced by the delay line at the front surface: $\phi_0(\beta) = \arg \tilde{W}_i(\beta)$. If no chirp was present, the function $\phi_0(\beta)$ would be a linear function. The spectrum of the source can be estimated from $\tilde{S}(\beta) = |\tilde{W}_i(\beta)|$.

To estimate the dispersion function $k = k(\beta)$ that maps between β and k, the periodicity in the medium, one computes the difference in the phase between the front and back reflections: $\phi_r(\beta) = \arg \tilde{W}_r(\beta) - \phi_0(\beta)$. The function $\phi_r(\beta)$ is then unwrapped by using a one-dimensional phase-unwrapping method. For this method, there must be no zeros in the functions $\tilde{W}_i(\beta)$ or $\tilde{W}_r(\beta)$ so that the phase is well defined. Furthermore, the signal cannot be undersampled, so that the phase difference between two samples of $\phi_r(\beta)$ is greater than π or less than $-\pi$. If these criteria have been satisfied then the estimate of $k(\beta) = \phi_r(\beta)/2d$, where d is the thickness of the slab. This function $k(\beta)$ may be used to resample $\tilde{W}(\beta)$ to $\tilde{W}(k)$.

In practice, one would likely want to fit the function $k(\beta)$ to a low-degree polynomial, rather than use a sampled version. This approach will be more noise robust if one knows that the dispersion of higher-order terms can be neglected.

5. Dispersion Correction in Stratified Media

A homogeneous medium can be characterized by a single dispersion function $k(\omega)$. If there are several different media, with known dispersion functions and layer thicknesses, the method for homogeneous media can be used to successively correct the dispersion of multiple layers beginning with the most shallow layer and working deeper. A medium with a depth-dependent dispersion will in general have a dispersion $k(\omega, z)$. In the optical approximation, the medium phase retardance function $\phi_S(\omega, z)$ is given by

$$\phi_S(z, \omega) = 2\int_0^z k(\omega, \zeta)\mathrm{d}\zeta. \tag{12}$$

A stratified medium can be defined as having N layers, each with its own dispersion $k_i(\omega)$, and with boundaries $z_i < z < z_{i+1}$ and $z_1 = 0$. Stratified dispersion could be represented as a piecewise linear approximation to a continuously varying dispersion. The dispersion of the stratified medium is

$$\begin{aligned}
\phi_S(z, \omega) &= 2(z - z_1)k_1(\omega) \qquad \text{for } z_1 < z < z_2 \\
\phi_S(z, \omega) &= 2(z - z_n)k_n(\omega) + 2\sum_{i=1}^{n-1}(z_{i+1} - z_i) \\
&\quad \times k_i(\omega) \qquad \text{for } z_n < z < z_{n+1}
\end{aligned} \tag{13}$$

Starting from an estimate of $\tilde{G}(\omega)$, the dispersion of each layer is iteratively corrected for increasing depths into the medium. To do so, the algorithm is first applied to the entire reflectance axial scan for the top-layer medium. Once the data corresponding to the first layer has been found, it can be zeroed so it no longer makes a contribution. The reflectance data is converted back to $\tilde{G}(\omega)$ and corrected for the second layer. This process is repeated for all the stratified layers. If the dispersion is assumed to be causal, there should be no reflectance artifacts from the deeper layers present in the more shallow layers. The algorithm for this method is listed in Table 3. Alternately, one can remove Step 6 by performing the translation in the spatial domain rather than in the frequency domain, yielding this simplified (but perhaps less accurate) procedure as specified in Table 4.

In addition, one can combine the two resamplings in Steps 6 and 1 in adjacent iterations to resample from $k_i(\omega)$ directly to $k_{i+1}(\omega)$, saving a calculation step, and omit the Steps 4–7 in the last iteration when $i = N$.

6. Envelope Demodulation and Speckle Reduction by Use of the Complex Analytic Signal

Once the estimate of $g(z)$ has been formed, one must interpret this data. A common strategy is to examine the magnitude of $g(z)$ to estimate the density of scattering at a particular point in an axial scan. This is frequently done by utilizing an envelope detector that rectifies and smoothes the signal magnitude. If the bandwidth is low, then a coherence length contains several optical cycles over which the magnitude can be averaged. Very short coherence lengths, however, contain only a few cycles. The envelope detector may then produce a noisy estimate of the signal reflectance. The complex analytic signal, however, produces a smoother estimate of the envelope by computing the quadrature component of the interference signal and including this in the magnitude estimate. Figure 1 shows two Gaussian wavepackets, one of which is envelope demodulated (a),

Table 4. Simplified Algorithm for Dispersion Correction in a Stratified Medium

1. Resample $\tilde{G}(\omega)$ to $\tilde{G}(k)$ by using the relation $k = k_i(\omega)$.
2. Take the inverse Fourier transform (via the FFT) to find $g_i(z)$.
3. Extract the region $0 < z < z_{i+1} - z_i$ out of $g_i(z)$, and translate the region $z > z_{i+1} - z_i$ over by a length z_{i+1} so it now starts at $z = 0$.
4. Zero out the portion of $g_i(z)$ for $z > z_n - z_{i+1}$ left vacant by the translation.
5. Take the Fourier transform (via the FFT) to find $\tilde{G}'(k)$.
6. Resample $\tilde{G}'(k)$ to $\tilde{G}'(\omega)$ by using the relation $k = k_i(\omega)$.
7. Increment i by one and go back to step 1 until $i > N$.

and the other of which is demodulated by the complex-analytic signal (b). The complex analytic signal removes the effect of the ac modulation.

There are also benefits in speckle reduction when the complex analytic signal is used. Most real objects will contain more detail than can be measured because the bandwidth of the source is too small to resolve features within a single coherence length. Because only the Fourier components present in the illumination can be measured, the envelope of the reflections appears to be modulated randomly, giving rise to the phenomenon known as speckle. While this work does not present a full analysis of the origins of speckle, this is discussed in more detail as it relates to OCT.[12,26–28] Speckle is unavoidable because a set of reflectors within a given coherence length may or may not reflect back light within the illumination bandwidth. However, randomly placed scatterers have a high probability of reflecting back some light. By using the complex analytic extension of the signal, the imaginary component of the interference signal can be inferred. The magnitude of the interference signal derived from this is less prone to be strongly modulated by speckle.

Figure 1 contains the probability distributions of the magnitude at a given point on an axial scan that can be expected when both types of demodulators are used to demodulate the signal from a randomly situated collection of point reflectors with Gaussian distributed scattering amplitudes. The envelope detector, because it detects the magnitude of the real part of the signal, has a half-normal distribution, with a mean-to-standard deviation ratio [signal-to-noise ratio (SNR)] of 1.32. The complex-analytic signal demodulator produces a Rayleigh distributed magnitude estimate, with a SNR of 1.91. This benefit occurs because the reflectance of a large collection of randomly placed Gaussian amplitude scatterers is a complex Gaussian random variable, with independent real and imaginary components. The benefit also occurs because the envelope demodulator, without smoothing, does not utilize nearby points for its

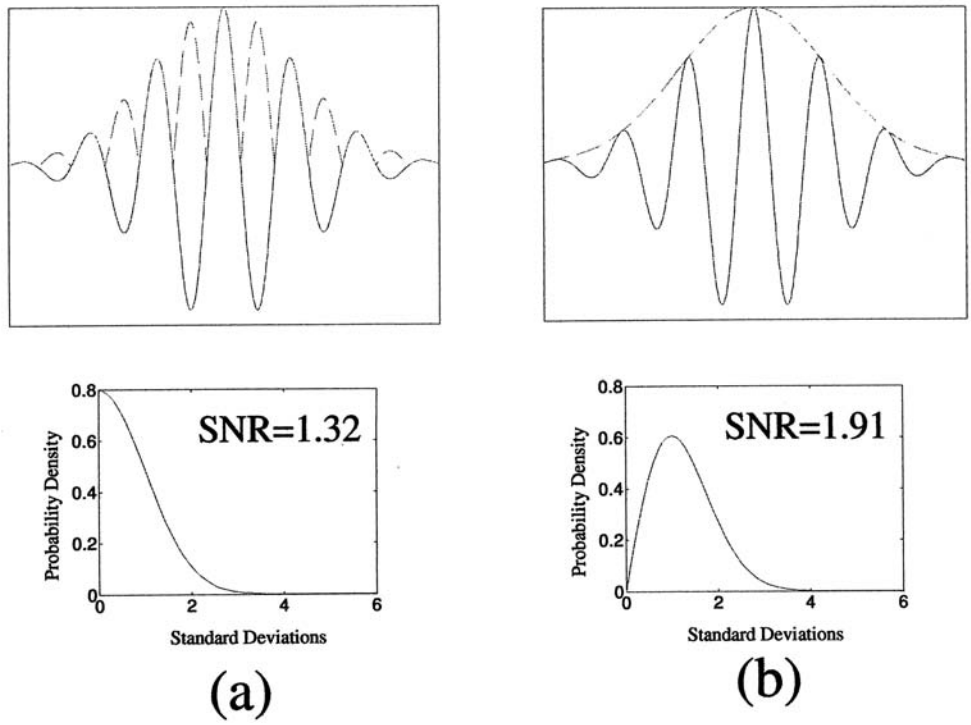

Fig. 1. Comparison of Gaussian wavepackets filtered with (a) the envelope detector, (b) the magnitude of the complex-analytic signal. Below are the probability distributions corresponding to finding a reflectance signal with a given magnitude, (a) half-normal distribution, (b) Rayleigh distribution, with their corresponding SNR.

magnitude estimate. Smoothing, however, may not be as useful when the bandwidth is too high to average over many optical cycles. The complex analytic signal forms a better pointwise estimate and is easy to compute when one already possesses the Fourier transform of the signal.

7. Experimental Demonstration

To demonstrate the application of this algorithm on experimental data, a stack of transparent layers was imaged with OCT. The top layer consisted of PDMS (polydimethylsiloxane) while the underlying layers were glass slides separated by small air gaps created by placing adhesive tape between the slides. The dispersion of the PDMS and the glass media caused group velocity dispersion that broadened the point-spread function (PSF) by depth-dependent amounts. We used the FFT-based method to correct the depth in the glass and the PDMS layers to produce transform-limited resolution at all depths.

Our OCT system consisted of a passively mode-locked Ti–sapphire laser with a center wavelength of 800 nm generating 100 fs pulses at a rate of 80 MHz with 500 mW average power. By sending the pulses through a narrow-core high-index silica/germania fiber, the spectrum was broadened through nonlinear continuum generation to approximately 80 nm FWHM bandwidth between 760 and 840 nm.[21] Dispersion is noticeable in the glass and the PDMS for scan depths larger than 1 mm. However, most of the dispersion was caused by the visible-wavelength achromatic lens used to focus the OCT beam. The achromat was used to make the focal length of the lens more uniform as a function of wavelength. When using a chromatically uncorrected lens, we found the spectral reflectance from various depths to be highly nonuniform, which degraded the resolution along the axial scan. Fortunately, the resulting dispersion of the lens was easily corrected by use of the present algorithm. The remainder of the OCT system was implemented with fiber optics that itself, can introduce additional chirp. The delay line consisted of a retroreflecting mirror scanned along an arc by a galvanometer-rotated arm. The recombined signal was sampled on a silicon photodetector.

Because the retroreflector was on a rotating rather than a translating arm, the angular movement did not correspond to a linear path delay. For this delay line, the delay nonlinearity $r(t) = R \sin t$, where R is the radius of the delay-line arm, and the dispersion function is $\phi_1(\omega) = \omega/c$, where c is the speed of light. Because the delay-line function is odd, the second-order term is zero and was approximated by a linear function $r(t) = Rt$. Therefore no resampling was required when moving from $P(t)$ to $P(t')$.

The data taken were 500,000 samples of the interference signal for each axial scan, which corresponded to samples of the function $f(t)$. Seven reflections dominated the reflectance signal, which can be seen in Fig. 2. Figure 2 is a low-resolution image of the stack. The top reflection denoted by (a, b) is an air–PDMS interface. The second reflection

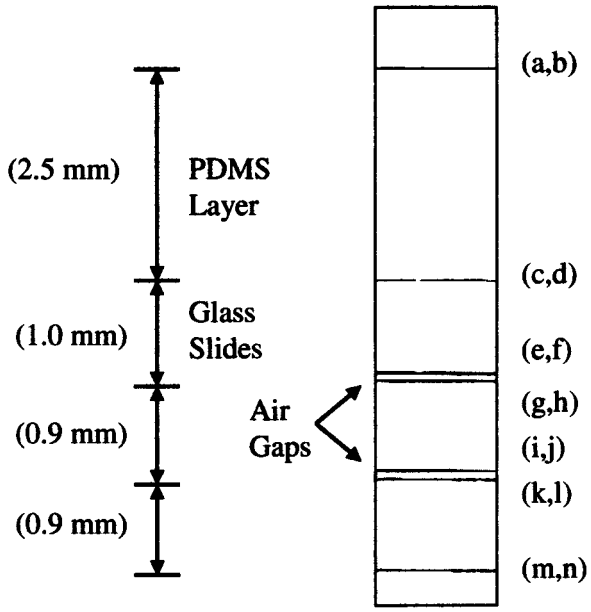

Fig. 2. Low-resolution OCT image of the PDMS/glass stack. Letters refer to axial scan data shown in Figs. 4 and 5.

(c, d) is a PDMS–glass interface, and the other five reflections are glass–air interfaces. The thicknesses of the layers are shown in the figure.

A number of parameters were required to apply the algorithm, which can be divided into two categories: dispersion-dependent and spectrally-dependent components. The spectrally-dependent components consisted of the power spectrum of the source and the noise spectrum due to the random photon arrivals. Both were estimated by averaging the magnitude of the Fourier-transform of 30 axial scans. The spectrum smoothed with a 10-nm wide convolution filter to remove ripples in the spectrum due to the placement of the layers. This spectrum estimates the sum of the noise and the source power-spectral density. We then estimated the noise power spectral density by averaging the power-spectral density over a range of frequencies in the visible wavelength range outside of the source spectrum. We experimentally found the noise spectrum to be white with only a variation of approximately 10%. This noise estimate was subtracted from the total spectrum to estimate the source spectrum $\bar{S}(\omega)$, with negative values set to zero. A modified spectrum was then calculated by use of Eq. (8). Figure 3 shows the Gaussian-line original source spectrum and the modified nearly flat spectrum.

We note that in the standard implementation of OCT, it is desirable to achieve a Gaussian source spectrum. We have chosen to digitally modify a Gaussian source spectrum to improve our resolution. A Gaussian spectrum is chosen because it produces a Gaussian point-spread function with long tails but no sidelobe maxima. However, we note two reasons why this may not be desirable. First, the source bandwidth is usually finite so a true Gaussian shape can never be fully realized. More importantly, in-

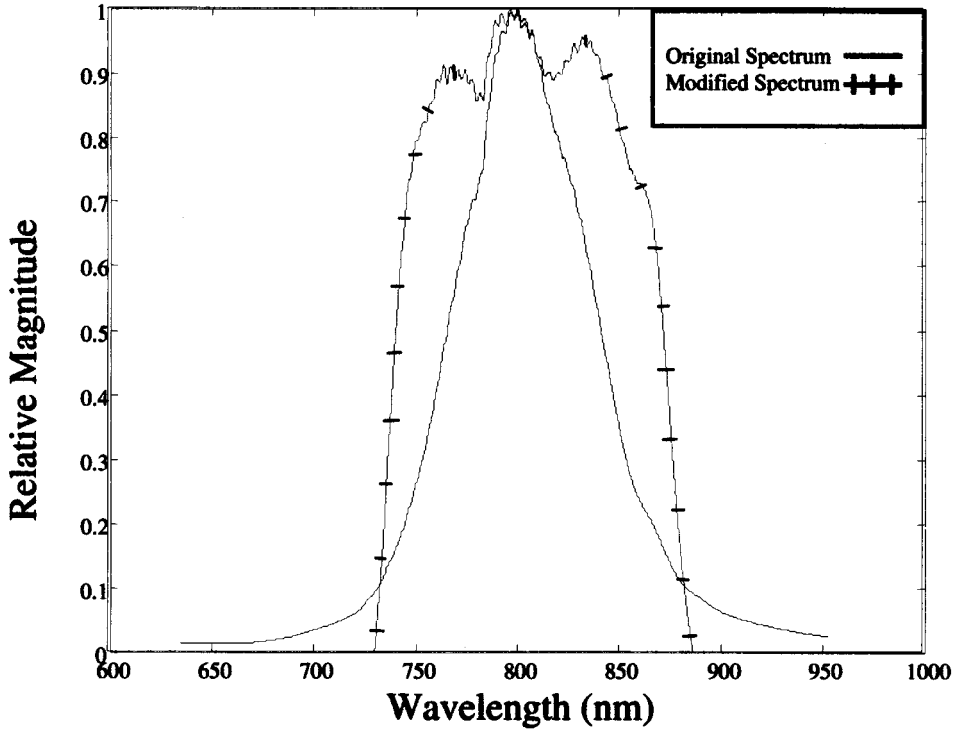

Fig. 3. Source spectrum and modified spectrum in OCT image.

sistence on the Gaussian shape disregards improvements that can be made based on the number of photons that are captured. With a high photon count, even relatively weak frequencies can yield useful resolution, while conversely at low photon count one must not overemphasize the tails of the Gaussian spectrum. The linear least-squares estimator of Eq. (8) both rejects noise outside of the wavelengths of interest and makes the spectrum more uniform. However, least-squares estimates tend to heavily penalize deviation due to noise. The noise penalty and flat spectrum both contribute to produce considerable sidelobes to the point-spread function. In this paper, we minimized the effect of the sidelobes by adding +10 dB to our noise estimate. However, in future work we will explore windowing functions that can be applied to a finite, nearly-flat spectrum that can minimize sidelobes, such as the prolate-spheroidal windows. An ideal window would permit the linear filter structure of Eq. (8) to be modified so that it could still be carried out by linear convolutions on digital signal processing hardware.

The dispersion parameters can be split into four components: the fixed dispersion caused by the differences between the sample and delay arms in the interferometer, the dispersion caused by the delay mechanism, the dispersion of the PDMS, and the dispersion of the glass. Because of the wide bandwidth, both quadratic and cubic chirp parameters must be fit to achieve good results. Because the delay mechanism occurs in air, we neglected the delay-line dispersion. We fit six parameters (two for each interface) to minimize the PSF at the air–PDMS interface, glass–PDMS interface, and the bottom glass–air interface, and applied the algorithm of Section 6. The fixed dispersion was fit by minimizing the air–PDMS reflection width. The PDMS dispersion was fit by then minimizing the glass–PDMS reflection width, and the glass dispersion was fit by then minimizing the glass–air bottom reflection width. Multiple iterations of the algorithm with trial parameters were required to fit the six parameters. The majority of the dispersion was due to the achromat lens and therefore was corrected at the top surface, but considerable dispersion occurred at deeper layers, enough to require correction.

To implement the algorithm, we utilized the approximate prolate-spheroidal bandlimiting interpolator.[29] Once the source and noise spectrum were estimated, and the chirp parameters were fit by minimizing the PSF at each of the three interfaces, the inversion algorithm based on the second algorithm of Section 6 was carried out with the procedure outlined in Table 5.

The results of this procedure are shown in Figs. 4 and 5. The letters next to each graph indicate the interface (Fig. 2) where each reflection occurred. The graphs a, c, f, g, i, k, and m are the original uncorrected PSF, and the others are corrected. While the amount of quadratic and cubic chirp were depth and material dependent, this procedure has made each of the corrected PSFs nearly transform limited with a 2- or 3-micrometer width. The width of the reflections in f, h, j, and l indicate that the procedure is performing well because they are nearly bandwidth limited despite the fact that they were not

Table 5. Procedure for Dispersion Correction in PDMS–Glass Stack

1. The temporal signal $P(t)$ underwent a Fourier transform to find $\tilde{P}(\omega)$.
2. The Weiner filter estimate of $\tilde{G}(\omega)$ was found from $\tilde{P}(\omega)$.
3. The space-invariant component of the chirp was multiplied into the Fourier spectrum to minimize the width of the top reflection.
4. The function $\tilde{G}(\omega)$ was resampled to the spatial coordinates $\tilde{G}(k)$ by using the dispersion parameters fit to the PDMS.
5. $\tilde{G}(k)$ underwent an inverse-Fourier transform to yield $g(z)$.
6. The data for the first and second reflection was copied out of $g(z)$ as the corrected results.
7. The function $g(z)$ was translated to move the second reflection to $z = 0$, and the rightmost portion of $g(z)$ was set to zero.
8. The function $g(z)$ was Fourier transformed to $\tilde{G}'(k)$.
9. $\tilde{G}'(k)$ was resampled with the dispersion parameters fit to the glass to yield $\tilde{G}''(k)$.
10. $\tilde{G}''(k)$ was inverse-Fourier transformed to produce $g''(z)$.
11. The rest of the reflections in the glass were extracted from $g''(z)$ to provide the other five PSFs.

specifically corrected for the purpose of fitting the dispersion parameters. While each of the graphs have been normalized, there was also a corresponding increase in the magnitude of each of the corrected PSFs that improves visibility of the data.

Figure 6 shows the experimentally measured dispersion of the PDMS and the glass from an OCT line scan. The dispersion is measured with the group velocity component removed as a function of the phase shift at each wavelength. The procedure of Section 4 was used to calibrate this chirp. To compute the dispersion of the 2.5 mm of PDMS, the reflections at the PDMS–air and PDMS–glass interfaces were isolated, Fourier transformed, and their phases subtracted from each other. The same procedure was done with the PDMS–glass and bottom glass–air reflection, which contained 2.9 mm of glass thickness with 0.1 mm of air. The phase difference was then unwrapped, which adds integer multiples of 2π to remove phase discontinuities. The glass appears to have somewhat more chirp than the PDMS. The ripples in the phase at the extremes of the spectrum are due mostly to the lower signal at those wavelengths, and the truncation of the chirped signals because they occupied a range of the axial scan that slightly blurred into the adjacent reflections. The dispersion of materials can be both characterized by OCT and corrected digitally.

8. Discussion

The degree of dispersion is sensitive to the quality of the fit of the dispersion parameters, making it a challenge to find the optimal combination. A similar sensitivity exists when attempting to correct the dis-

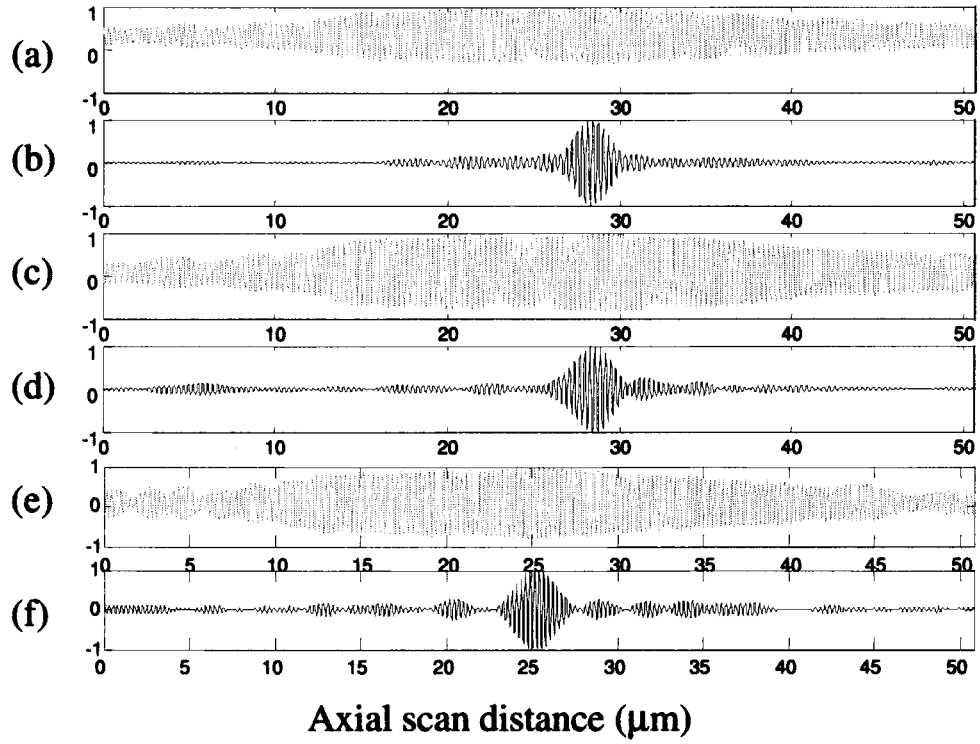

Fig. 4. Detail of sections of axial scan corresponding to air–PDMS and glass–PDMS boundaries. The corrected scans (b, d, f) are significantly narrower than the original scans (a, c, e), providing an enhancement in axial imaging resolution. Letters refer to boundaries as labeled in Fig. 2.

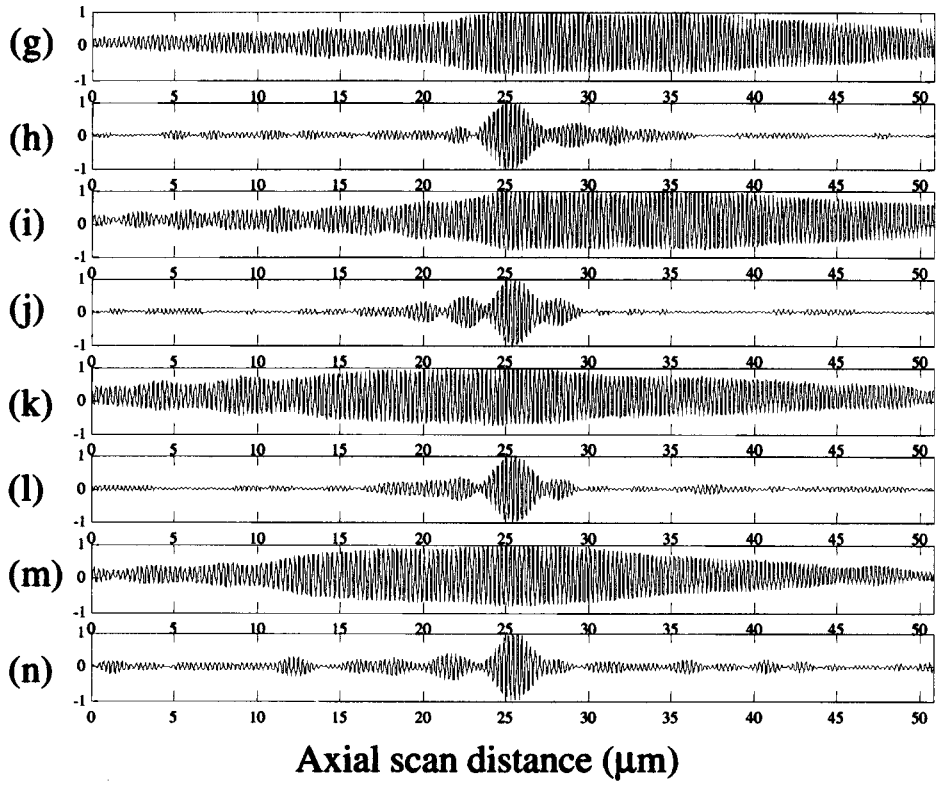

Fig. 5. Detail of sections of axial scan corresponding to glass–air boundaries. The corrected scans (h, j, l, n) are significantly narrower than the original scans (g, i, k, m), providing an enhancement in axial imaging resolution. Letters refer to boundaries as labeled in Fig. 2.

persion by use of optical balancing, especially if one attempts to balance it over a long axial scan range. The benefit of digital processing is that the dispersion correction can be changed dynamically without having to re-acquire data or change the optical system whatsoever. Our correction of dispersion utilizes a parameterized model that corrects second- and third-order dispersion. If higher bandwidth sources are used, it can be expected that more terms will be needed to achieve bandwidth-limited resolution. Because the major constituent of most tissues is water, we expect that correction for the dispersion of water will improve resolution. Other absorbers that are expected to influence dispersion are lipids and oxy/deoxyhemoglobin. Without accounting for the contents of the tissue, however, high resolution at large depths can be expected to suffer with large bandwidth illumination. We believe that automatic fitting of the chirp parameters is possible because the unchirped version of data is readily recognizable, and we are pursuing this strategy. While distinct interfaces as shown here are not likely to be present in most tissues, tissue is not completely uniform and does contain strong scatterers that can be used to determine if dispersion correction is achieved.

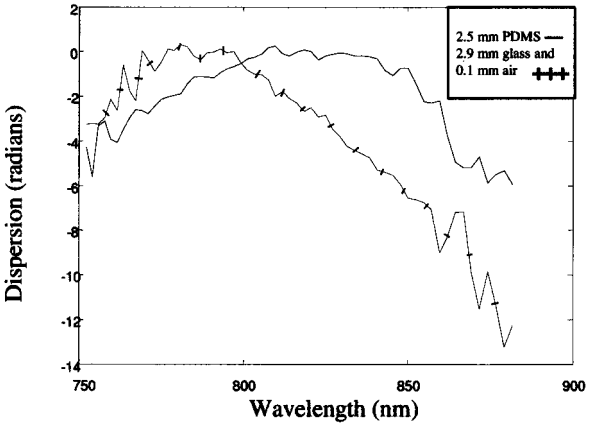

Fig. 6. Measured dispersion in PDMS and glass.

When acquiring OCT data it may be desirable in practice to intentionally introduce chirp into the signal. Adding chirp does not degrade the SNR because the noise is discriminated from signal by its frequency content, which is left unchanged by adding chirp. The benefit of chirp is to disperse the PSF over a wider length of the axial scan. This conserves the dynamic range of the quantization mechanism. A typical analog-to-digital converter has 8 to 16 bits of dynamic range. If all of the chirp is removed before quantization, then the dynamic range will need to span the maximum amplitude of the signal. Often images have strong reflectors that will saturate the electronic signal amplifier. However, a chirped signal will lower the maximum amplitude of the signal, permitting further amplification before quantization and more fully utilizing the dynamic range.

With these methods, it is critical to avoid nonlinearities, including distortions from portions of the signal that do not fit within the sampling range of the digitizer. Nonlinearities will introduce ghost images that will clutter the true reflectance estimate. Adding chirp can help conserve dynamic range and therefore avoid this problem.

9. Conclusion

Dispersion is a linear distortion that degrades the quality of optical coherence tomography images, but does not reduce the received signal. The algorithm presented here applies digital postprocessing to invert the linear distortion of the received signal and produce a corrected image that achieves bandwidth-limited axial resolution. The estimate of the scattering incorporates the delay-line and material dispersion, source spectrum, detector quantum efficiency, and integration time. We demonstrate this technique to measure the dispersion and correct the image of a PDMS–glass dielectric layer stack.

Ultrahigh bandwidth Ti–sapphire oscillators and amplified doped fiber sources will produce wide spectra that will suffer more from dispersion. In biological tissues,[30,31] the presence of absorbers such as hemoglobin and water will also increase dispersion. Optical correction of dispersion can partially compensate for the problem, but is difficult to achieve over a long axial scan range. Digital correction of the chirp can flexibly fix remaining problems. With additional algorithms to estimate the chirp parameters from the image, digital correction can be done automatically and become an integral part of OCT image acquisition and enhancement.

We acknowledge the scientific contributions of Alex Schaefer for his work on developing a digital OCT acquisition system and software. This research was supported by the National Science Foundation (BES-0086696), the Whitaker Foundation, and the Beckman Institute for Advanced Science and Technology.

References

1. D. Huang, E. A. Swanson, C. P. Lin, J. S. Schuman, W. G. Stinson, W. Chang, M. R. Hee, T. Flotte, K. Gregory, C. A. Puliafito, and J. G. Fujimoto, "Optical Coherence Tomography," Science **254,** 1178–1181 (1991).
2. B. E. Bouma and G. J. Tearney, eds., *Handbook of Optical Coherence Tomography* (Marcel Dekker, Inc., New York, 2001).
3. J. G. Fujimoto, S. A. Pitris, S. A. Boppart, and M. E. Brezinski, "Optical coherence tomography: an emerging technology for biomedical imaging and optical biopsy," Neoplasia **2,** 9–25 (2000).
4. S. A. Boppart, B. E. Bouma, C. Pitris, J. F. Southern, M. E. Brezinski, and J. G. Fujimoto, "In vivo cellular optical coherence tomography imaging," Nat. Med. (N.Y.) **4,** 861–864 (1998).
5. G. J. Tearney, M. E. Brezinski, B. E. Bouma, S. A. Boppart, C. Pitris, J. F. Southern, and J. G. Fujimoto, "In vivo endoscopic optical biopsy with optical coherence tomography," Science **276,** 2037–2039 (1997).
6. J. F. de Boer, T. E. Milner, M. J. C. van Germert, and J. S. Nelson, "Two-dimensional birefringence imaging in biological tissue by polarization sensitive optical coherence tomography," Opt. Lett. **22,** 934–936 (1997).
7. J. A. Izatt, H.-W. Kulkarni, K. Wang, M. W. Kobayashi, and M. W. Sivak, "Optical coherence tomography and microscopy in gastrointestinal tissues," IEEE J. Selected Top. Quantum Electron. **2,** 1017–1028 (1996).
8. J.-C. Diels and W. Rudolph, *Ultrashort Laser Pulse Phenomena* (Academic, San Diego, Calif., 1996).
9. A. Kohlhaas, C. Fromchen, and E. Brinkmeyer, "High resolution OCDR for testing integrated-optical waveguides: Dispersion-corrupted experimental data corrected by a numerical algorithm," J. Lightwave Technol. **9,** 1493–1502 (1991).
10. E. Brinkmeyer and R. Ulrich, "High-Resolution OCDR in dispersive waveguides," Electron. Lett. **26,** 413–414 (1990).
11. A. F. Fercher, C. K. Hitzenberger, M. Sticker, R. Zawadzki, B. Karamata, and T. Lasser, "Numerical dispersion compensation for Partial Coherence Interferometry and Optical Coherence Tomography," Opt. Express **9,** 610–615 (2001).
12. K. M. Yung, S. L. Lee, and J. M. Schmitt, "Phase-domain processing of optical coherence tomography images," J. Biomed. Opt. **4,** 125–136 (1999).
13. J. M. Schmitt, "Restoration of optical coherence images of living tissue using the clean algorithm," J. Biomed. Opt. **3,** 66–75 (1998).
14. J. M. Schmitt and A. Knuttel, "Model of optical coherence tomography of heterogeneous tissue," J. Opt. Soc. Am. A **14,** 1231–1242 (1997).
15. Y. Pan, R. Birngruber, and R. Engelhardt, "Contrast limits of coherence-gated imaging in scattering media," Appl. Opt. **36,** 2979–2983 (1997).
16. A. F. Abouraddy, M. B. Nasr, B. E. A. Saleh, A. V. Sergienko, and M. C. Teich, "Quantum-optical coherence tomography with dispersion cancellation," Phys. Rev. A **65,** 053817-1–053817-6 (2002).
17. X. Clivaz, F. Marquis-Weible, and R. P. Salathe, "Optical low coherence reflectometry with 1.9 micron spatial resolution," Electron. Lett. **28,** 1553–1555 (1992).
18. B. E. Bouma, G. J. Tearney, S. A. Boppart, M. R. Hee, M. E. Brezinski, and J. G. Fujimoto, "High resolution optical coherence tomographic imaging using a modelocked Ti:A1203 laser," Opt. Lett. **20,** 1486–1488 (1995).
19. W. Drexler, U. Morgner, F. X. Kartner, C. Pitris, S. A. Boppart, X. Li, E. P. Ippen, and J. G. Fujimoto, "In vivo ultrahigh resolution optical coherence tomography," Opt. Lett. **24,** 1221–1223 (1999).
20. B. E. Bouma, G. J. Tearney, I. P. Bilinsky, B. Golubovic, and J. G. Fujimoto, "Self-phase-modelocked Kerr-lens mode-locked Cr:forsterite laser source for optical coherence tomography," Opt. Lett. **21,** 1839–1841 (1996).
21. D. L. Marks, A. L. Oldenburg, J. J. Reynolds, and S. A. Boppart, "Study of an ultrahigh numerical aperture fiber continuum generation source for optical coherence tomography," Opt. Lett. **27**, 2010–2012 (2002).
22. J. D. Jackson, *Classical Electrodynamics* (Wiley, New York, 1975).
23. M. Bertero and P. Bocacci, *Introduction to Inverse Problems in Imaging* (IOP Publishing, Philadelphia, 1998).
24. M. Born and E. Wolf, *Principles of Optics* (Cambridge University, Cambridge, UK, 1980).
25. L. Mandel and E. Wolf, *Optical Coherence and Quantum Optics* (Cambridge University, Cambridge, UK, 1995).
26. M. Bashkansky and J. Reintjes, "Statistics and reduction of speckle in optical coherence tomography," Opt. Lett. **25,** 545–547 (2000).
27. J. M. Schmitt, S. H. Xiang, and K. M. Yung, "Speckle in Optical Coherence Tomography," J. Biomed. Opt. **4,** 95–105 (1999).
28. J. Rogowska and M. E. Brezinski, "Evaluation of the Adaptive

Speckle Suppression Filter for Coronary Optical Coherence Tomography Imaging," IEEE Trans. Med. Imaging **14,** 1261–1266 (2000).
29. J. J. Knab, "Interpolation of band-limited functions using the approximate prolate series," IEEE Trans. Inf. Theory **IT-25,** 717–720 (1979).
30. S. A. Boppart, G. J. Tearney, B. E. Bouma, J. F. Southern, M. E. Brezinski, and J. G. Fujimoto, "Noninvasive assessment of the developing Xenopus cardiovascular system using optical coherence tomography," Proc. Natl. Acad. Sci. USA **94,** 4256–4261 (1997).
31. J. M. Schmitt, M. J. Yadlowsky, and R. F. Bonner, "Subsurface imaging of living skin with optical coherence microscopy," Dermatology **191,** 93–98 (1995).